ELSEVIER

Nuclear Physics A 671 (2000) 71–95

NUCLEAR PHYSICS A

www.elsevier.nl/locate/npe

Covariance analysis of selection rules governing the $\gamma-$ decay cascades of the rotational nucleus ^{164}Yb

S. Leoni [a], T. Døssing [b], A. Bracco [a], S. Frattini [a], G. Montingelli [a], E. Vigezzi [a], M. Bergström [b], G.B. Hagemann [b], B. Herskind [b], M. Matsuo [c]

[a] *Dipartimento di Fisica, Università di Milano, and INFN sez. Milano, Via Celoria 16, 20133 Milan, Italy*
[b] *The Niels Bohr Institute, Blegdamsvej 17, Copenhagen DK-2100 Ø, Denmark*
[c] *Yukawa Institute for Theoretical Physics, Kyoto University, Kyoto 606-8502, Japan*

Received 28 October 1999; received in revised form 13 December 1999; accepted 14 December 1999

Abstract

The γ-cascades feeding specific intrinsic configurations of ^{164}Yb are studied making use of a statistical analysis of counts fluctuations in γ–γ coincident spectra. In particular, variance and covariance spectra are obtained starting from the measured $(0,+)$, $(0,-)$ and $(1,-)$ gate-selected matrices. The analysis of the first ridge of the spectra yields about 25 excited bands carrying rotational energy correlations for the total spectrum, and about 10 in coincidence with each of the (α,π) configurations. The covariance of count fluctuations between the different (α,π) gates is expressed by an experimental correlation coefficient, r, which measures the degree of sharing of decay paths through the excited bands, and thereby the extent to which selection rules are obeyed by the decay. The correlation coefficient is around $r \approx 0.3$ for the ridge, and also in general rather small for valley fluctuations. Only at the highest valley energies, a tendency to larger correlation coefficients is seen, indicating some weakening of the selection rules over longer decay cascades. The results of the experimental analysis are compared to rotational damping model predictions based on cranked shell model plus residual interactions, and rather good agreement is found.

PACS: 21.10.Re; 21.60.Ka; 23.20.Lv; 27.60.+q
Keywords: Nuclear reaction ^{138}Ba(^{30}Si,4n) ^{164}Yb; $E_b = 140$, 145, 150, 155 MeV; Measured E_γ, γ–γ coincidence; Rotational continuum; Statistical analysis methods; Deduced properties of feeding transitions for high spin levels

1. Introduction

In recent years a considerable effort has been made to investigate the properties of the rotational motion of thermally excited nuclei. At rather low heat energy, excited regular bands carrying strong E2 transitions are found, while with increasing heat energy, the

0375-9474/00/$ - see front matter © 2000 Published by Elsevier Science B.V. All rights reserved
PII: S0375-9474(99)00842-8

bands are gradually dissolving and the collective E2 strength out of each state spreads over several transitions [1,2]. This spreading of the E2 strength implies a damping of the rotational motion at higher heat energies. With present day techniques, individual γ-rays emitted from such states are too weak to be resolved and placed in a level scheme, and our knowledge of damped rotation stems from analysis of unresolved coincidence spectra. Displaying such double coincidence energy spectra in an $E_{\gamma_1} \times E_{\gamma_2}$ plane, transitions along regular bands are separated from damped transitions, forming a landscape of ridges and valleys [3]. In particular, a statistical analysis of the count fluctuations allows to extract the number of excited bands, as well as the effective number of damped transitions [4,5]. The results of the fluctuation analysis are found to be well in accordance with a model of the thermally excited states as obtained from cranked mean bands interacting via two-body residual interactions [2]. Especially, simulations of decay cascades on the basis of this model produce spectra of approximately the same shape, carrying quantitatively the same count fluctuations in the different regions of the spectra as seen experimentally [6]. These results were obtained analyzing inclusive γ–γ spectra.

Further insight into the damping mechanism requires exclusive studies based on higher fold coincidences, in which either a configuration selection [7], or a multidimensional rotational correlation can be made [8]. In the first case the γ-cascades feeding into low-K and high-K bands of the nucleus ^{163}Er were studied with the aim of determining the validity of selection rules in the γ-cascades. In the second case, for the nucleus ^{168}Yb, fluctuations on the ridges in three dimensions, within an $E_{\gamma_1} \times E_{\gamma_2} \times E_{\gamma_3}$ cube, have been investigated. This provided information on the lengths of excited rotational bands, probing in more detail the strength of the residual interaction.

In the present paper we focus on the fluctuation analysis of the unresolved rotational transitions feeding different low-lying configurations of ^{164}Yb. By analyzing fluctuations on the ridges of the gated spectra, we deduce the effective number of excited bands, which feed into the different configurations. Additional information on the transitions feeding into the low-lying rotational bands is provided by analyzing the *covariance* between spectra gated by different bands. For the ridges, the statistics is good enough to check the consistency between the gated and total spectra, expressed as a sum rule, which is verified for the first time.

A covariance analysis of the measured spectra is carried out also in the valley regions, to determine how similar are the cascades feeding from the damped region into different configurations. The similarity is expressed through the *correlation coefficient*, in which the covariance between spectra is normalized in a proper way by the fluctuations of the individual spectra. This may shed light on the γ transitions, which bring the nucleus from the chaotic compound nucleus region [9,10], described by random combinations of the available configurations, into the zero temperature region, characterized by regular ordered motion, with selection rules and complete sets of quantum numbers for every state [11].

The experimental results are compared to the predictions based on cranked shell model calculations including a two-body residual interaction [2].

For completeness, Appendix A of the present paper contains the mathematical derivations of the correlation coefficient and its error bar. Especially, the first steps of the derivation demonstrate how the correlation coefficient directly measures the similarity of cascades.

2. The experiment and the data reduction

A high statistics, high fold data set on ^{164}Yb has been obtained through the reaction $^{30}Si + ^{138}Ba \rightarrow ^{168}Yb$, after 4n evaporation. The experiment was carried out at the Institut de Recherches Subatomiques of Strasbourg, using the Vivitron tandem accelerator and the multidetector system EUROGAM II. Two targets, each evaporated on a thin Au foil of $\approx 580\ \mu g/cm^2$, were used, with a total ^{138}Ba thickness of 450 $\mu g/cm^2$. The data were collected at 4 different beam energies $E_b = 140$, 145, 150 and 155 MeV, corresponding to a recoil velocity v/c of approximately $1.67 \pm 0.05\%$, for a study of the excitation function [12]. A total of 620×10^6 triple and higher-fold events (with an average Ge-fold of 5) was collected, out of which more than 60% was in average leading to ^{164}Yb as the final nucleus. Energy-dependent time gates on the Ge time signal were used to suppress background from neutrons.

For the purpose of the present analysis the data taken at different beam energies have been added together, after a proper individual Doppler shift correction, and several γ–γ spectra have been sorted according to the ‘‘spike-free’’ procedure described in Ref. [13].

At first, an high resolution γ–γ matrix with 0.5 keV/ch was constructed for a preliminary analysis of the level scheme [14] by the Radware software programs [15]. Fig. 1 shows the excitation energy relative to a rigid rotor (a) and the relative intensity population (b) of the ground state band (g-band) and of the four low-K basic signature and parity configurations $(\alpha,\pi) = (0,+)$, $(0,-)$, $(1,+)$ and $(1,-)$ of ^{164}Yb, as function of spin, as obtained from the analysis of the data. One can notice the weak intensity of the $(1,+)$ configuration as compared with the other three rotational bands, as a consequence of its higher excitation energy.

In addition, the data have been sorted into a number of γ–γ high resolution matrices (0.5 keV/ch), according to different gating requirements on the γ-ray energies. First, a two-dimensional (2D) spectrum collecting the entire decay flow of ^{164}Yb (Total matrix) has been obtained by gating on the lowest lying transitions of the g-band (indicated by closed circles in Fig. 1). Second, three γ–γ coincident spectra have been created by gating on high spin transitions which exclusively select the configurations $(\alpha,\pi) =$

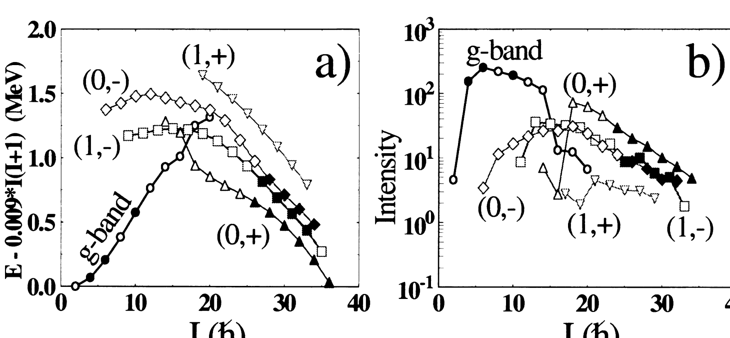

Fig. 1. Excitation energy relative to a rigid rotor (a) and relative intensity population (b) of the g-band and of the four lowest signature and parity configurations $(\alpha,\pi) = (0,+)$, $(0,-)$, $(1,+)$ and $(1,-)$ of ^{164}Yb, as function of spin. The closed symbols correspond to the transitions used as gates sorting the corresponding $\gamma-\gamma$ spectra.

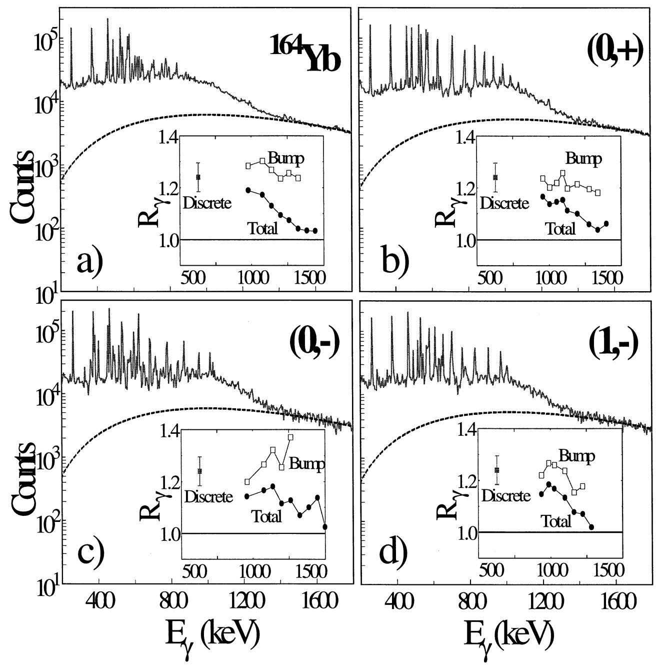

Fig. 2. One-dimensional spectra of ^{164}Yb obtained by gating on transitions of the g-band (a) and of the intrinsic configurations $(\alpha,\pi)=(0,+)$, $(0,-)$ and $(1,-)$ (b), (c) and (d). The dashed lines correspond to an extrapolation of the statistical E1 tail by the function $E_\gamma^3\exp(-E_\gamma/T)$, with $T\approx 0.34$ MeV. The insets of the figures show the anisotropy R_γ of the total spectrum (closed circles), of the continuum bump (open squares) and of purely stretched E2 low spin discrete transitions of ^{164}Yb (closed squares).

$(0,+)$, $(0,-)$ and $(1,-)$, as shown in Fig. 2 by closed symbols. Due to the low intensity of the $(1,+)$ rotational band, the γ–γ spectrum gated by this configuration could not be obtained with significant statistics.

As described in Appendix A, the gated spectra, named $C(E_{\gamma_1},E_{\gamma_2})$, are corrected for the background under the gate-selected peaks by subtracting properly normalized spectra, named $B(E_{\gamma_1},E_{\gamma_2})$, obtained by narrow gates around the peaks. The statistics collected in the background subtracted spectra

$$A_{\mathrm{b.s.}}\left(E_{\gamma_1},E_{\gamma_2}\right)=C\left(E_{\gamma_1},E_{\gamma_2}\right)-gB\left(E_{\gamma_1},E_{\gamma_2}\right) \tag{1}$$

is given in Table 1 for each of the gates. The background reduction factor g, calculated as the ratio between the number of channels covered by the narrow gates on the peaks

Table 1
Statistics collected in the original gated matrices, indicated by C, and in the corresponding background subtracted spectra, indicated by $A_{\mathrm{b.s.}}$ (cf. Eq. (1)). The values of the background reduction factors g are also given

	g	Statistics C	Statistics $A_{\mathrm{b.s.}}$
Total	0.36	1.45×10^9	890×10^6
$(0,+)$	0.55	880×10^6	300×10^6
$(0,-)$	0.51	650×10^6	270×10^6
$(1,-)$	0.41	550×10^6	98×10^6

and on the corresponding background, is also given in the table. Finally, the Compton and other uncorrelated events still present in the 2D spectra are reduced by use of a COR treatment, with a scaling of the uncorrelated background subtraction by a factor of $\approx$ 0.5 [16].

3. Analysis of spectra

3.1. Unresolved energy spectrum in one dimension

A one-dimensional (1D) analysis of the spectra is first performed in order to study the general features of the γ-ray intensity distribution. Fig. 2a shows in logarithmic scale the total projection, corrected for the detector efficiency, of the background subtracted matrix collecting the entire decay flow of ^{164}Yb (named Total matrix in the previous paragraph), obtained by gating on low spin transition of the g-band (see Fig. 1a). As observed in previous works on nuclei of the same mass region and deformation [17], three main components can be recognized in the spectrum: (i) the strong discrete peaks of the yrast transitions of ^{164}Yb, extending up to $E_\gamma \approx 1$ MeV; (ii) the statistical E1 tail at energies $E_\gamma >$ 1.4 MeV, which is extrapolated over the entire energy region by the function $E_\gamma^3 \exp(-E_\gamma/T)$, with $T \approx 0.34$ MeV (dashed lines in the figure); (iii) a pronounced bump in the region $1 < E_\gamma < 1.4$ MeV, populated by damped transitions of stretched E2 character, as deduced from the measured angular anisotropy $R_\gamma(E_\gamma) = W(157°)/\langle W(90°)\rangle$. In this expression $W(\theta)$ is the intensity of the 1D spectrum measured at the angle θ, which for $\theta = 90°$ is obtained averaging over the angles 72°, 80°, 99° and 107°. The inset of Fig. 2a shows the measured anisotropy for the total spectrum (closed circles) and for the bump (open circles) obtained after subtracting the E1 contribution, assumed to be isotropic, from the total spectrum. As one can see, the anisotropy of the transitions of the bump is found to be ≈ 1.26, which is close to the average value 1.24 ± 0.06 obtained from the analysis of purely stretched-E2 discrete transitions of ^{164}Yb (closed square in the figure). This confirms the rotational character of the continuum bump observed in the total spectrum, in accordance with a recent measurement of the collectivity, which is found to be of the same magnitude ($\approx$ 200 W.U.) as for the low lying discrete rotational states [18].

Figs. 2b, c and d show the total projections efficiency corrected of the background subtracted matrices gated on the $(\alpha,\pi) = (0,+)$, $(0,-)$ and $(1,-)$ intrinsic configurations of ^{164}Yb, as shown in Fig. 1. The spectra, normalized in the transition energy region around 1.6 MeV, appear very similar to the total spectrum of Fig. 2a: besides the strong discrete peaks of the yrast transitions of the selected (α,π) configuration and the statistical E1 tail, a pronounced rather smooth bump can be clearly observed in the transition energy region $1 < E_\gamma < 1.4$ MeV. Again, angular distribution measurements, shown in the insets of the figures, indicate that the transitions of the bump have a stretched E2 character with an anisotropy $R_\gamma = 1.24 \pm 0.04$, which agrees with the value found for purely stretched E2 discrete transitions of ^{164}Yb.

In conclusion, the analysis of the general features of the 1D spectra gated by selected intrinsic configurations clearly shows the existence of a pronounced bump of rotational transitions, in coincidence with the different low-lying (α,π) structures. This encourages the investigation of the properties of the configuration dependence of the rotational motion even at excitation energies where the damping phenomenon dominates strongly.

3.2. Fluctuation analysis

The gated spectra are mainly analyzed in two dimensions, by statistical analysis methods. The fluctuations of counts in each channel of the two-dimensional background subtracted spectra $A_{\mathrm{b.s}}$, defined by Eq. (1) and listed in Table 1, are evaluated by the program STATFIT [5] and the corresponding statistical moments μ_1 and μ_2 are stored into 2D spectra, after the spectra have been compressed to 4 keV/ch and all pairs of resolved transitions are removed from the matrices, making use of the Radware programs [15]. This ensures a better evaluation of the fluctuations, which would be otherwise severely affected by the low lying intense transitions. Fig. 3 shows typical perpendicular cuts with a width $\Delta E_\gamma = 4\hbar^2/\Im^{(2)} \approx 60$ keV at the average transition energy $\langle E_\gamma \rangle = 900$ keV on the first moment μ_1 spectra of the Total and (α,π) gated matrices of ^{164}Yb. As one can see, each spectrum shows the ridge-valley pattern typical of well deformed rotational nuclei [5]. In particular, the arrows in the figure point to the first ridge structures populated by unresolved discrete rotational bands, which appear to be particularly weak as a consequence of the subtraction of the known intense discrete transitions.

The μ_1 and μ_2 fluctuation spectra are first used to extract the effective number of decay paths, which eventually will feed into the gate-selected band. The number $N^{(2)}_{\mathrm{path}}$ of decay paths having two γ transitions with energy lying in a given $4\hbar^2/\Im^{(2)} \times 4\hbar^2/\Im^{(2)} = 60 \times 60$ keV window of a COR background subtracted spectrum $A_{\mathrm{b.s.}}$ are obtained from the expression

$$N^{(2)}_{\mathrm{path}}(A_{\mathrm{b.s.}}) = \frac{N_{\mathrm{eve}}(A_{\mathrm{b.s.}})\,\mu_1(A_{\mathrm{b.s.}})}{\mu_2(A_{\mathrm{b.s.}}) - \tilde{\mu}_1(A_{\mathrm{b.s.}})} \times \frac{P^{(2)}}{P^{(1)}}. \quad (2)$$

As derived in Appendix A, in the denominator of (2) the subtraction of the first moment $\tilde{\mu}_1(A_{\mathrm{b.s.}})$, defined as

$$\tilde{\mu}_1(A_{\mathrm{b.s.}}) = \mu_1(C) + g^2\mu_1(B) \quad (3)$$

takes into account the fluctuations from the counting statistics of the original gated raw spectrum C as well as of the raw background spectrum B. In fact, the contribution to μ_2 given by the most interesting fluctuations, related to the nature of the finite number of transitions available to each decay cascade, is quadratic in the number of events, while the pure count fluctuations give a contribution to μ_2 which is linear in the number of events. In Eq. (3), $N_{\mathrm{eve}}(A_{\mathrm{b.s.}})$ is the number of events in the sector $4\hbar^2/\Im^{(2)} \times 4\hbar^2/\Im^{(2)}$ of the background subtracted spectrum $A_{\mathrm{b.s}}$, and the $P^{(2)}/P^{(1)}$ term corrects for the finite resolution of the detectors, as discussed in Ref. [5].

The average number of paths obtained from the analysis of the first ridge of the $(\alpha,\pi) = (0,+)$, $(0,-)$ and $(1,-)$ gated matrices is shown by open circles in the bottom of Fig. 4. It measures the effective number of discrete paths which eventually will feed into a given (α,π) gate-selected band, and the average is around 10, fairly independent of the $\gamma-$ray energy, and with no appreciable difference among the specific configurations. In contrast, a number of ≈ 25 paths (closed symbols in the figure) is obtained

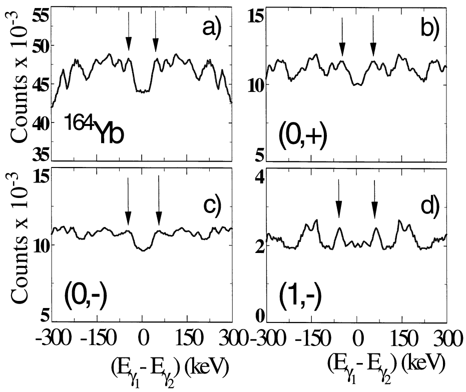

Fig. 3. Perpendicular cuts 60 keV wide at the average transition energy $\langle E_\gamma \rangle = 900$ keV on the first moment μ_1 spectra corresponding to the Total, $(0,+)$, $(0,-)$ and $(1,-)$ gated matrices of ^{164}Yb. The arrows point to the ridge structures populated by unresolved regular rotational bands.

from the analysis of the first ridge of the Total matrix selecting as final nucleus ^{164}Yb, in agreement with the systematic results previously obtained for nuclei of the same mass region [5].

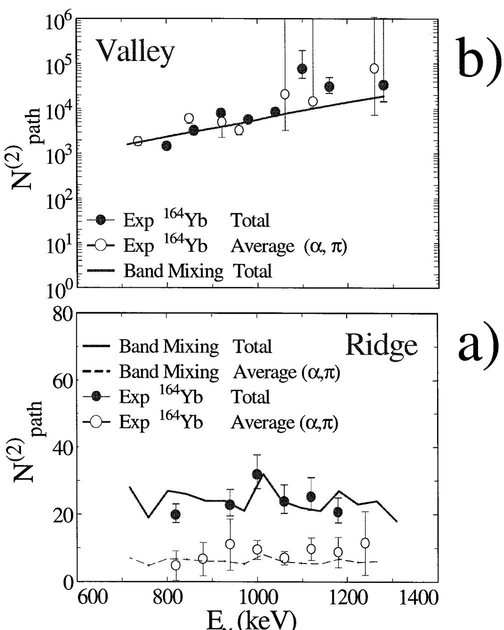

Fig. 4. The number $N^{(2)}_{\rm path}$ of paths extracted from the fluctuation analysis of the ridge (a) and of the valley (b) structures of the 2D matrices gated by specific intrinsic configuration of ^{164}Yb. The closed symbols refer to the analysis of the Total matrix, collecting the entire decay flow of the nucleus, while the open symbols correspond to the average values obtained from the study of 2D spectra gated by the intrinsic configurations $(\alpha,\pi) = (0,+)$, $(0,-)$ and $(1,-)$. The lines in the figures have been obtained from cranked shell model calculations including a two-body residual interaction of surface delta type [2].

The number of paths obtained from the analysis of the valley region is shown in the top part of Fig. 4 for both the Total spectrum of ^{164}Yb and the average over the $(\alpha,\pi) = (0,+)$, $(0,-)$ and $(1,-)$ gate-selected matrices. In both cases, a large number of paths, of the order of 10^4, is obtained from the valley fluctuations. This is in agreement with previous studies for the same mass region and deformation [5–7], and supports the assumption of rotational damping, according to which the valley should mostly collect damped transitions from states at which one expects the rotational decay to be fragmented. At high transition energies, the data show large error bars, as a consequence of two possible different effects: (i) the weakening of the E2 continuum in favor of E1 statistical transitions, as shown by the corresponding 1D spectra of Fig. 1; (ii) the poor counting statistics collected in the valley region of the 2D gated matrices. In fact, as shown in Fig. 5, a typical low resolution channel (4 keV/ch) of the background subtracted gated matrices $A_{b.s.}$, defined by Eq. (1), does not contain more than few hundred counts in the high transition energy region ($E_\gamma \geqslant 1$ MeV), especially when gating on specific (α,π) intrinsic configurations. This makes the statistical analysis of the valley very difficult, as it can be clearly seen in Fig. 6, where the ratio $\mu_2(A_{b.s.})/\mu_1(C)$ obtained from the fluctuation analysis of the valley of the Total and (α,π) gated spectra is shown as function of transition energy. As one can see, for $E_\gamma \geqslant$ 1 MeV the normalized fluctuations gradually approach 1 (solid line), which is the statistical limit obtained in the case of pure count fluctuations, as discussed in Appendix A in connection with Eq. (A.18).

3.3. Covariance analysis

The study of the counts fluctuations of 2D spectra, as discussed in the previous section, has allowed to investigate the average properties of the rotational motion built on specific (α,π) configurations. More detailed information can be obtained by the

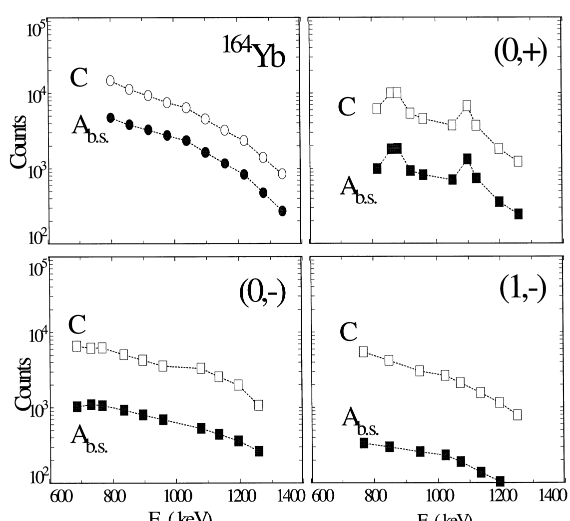

Fig. 5. The number of counts collected in a 4 keVx4 keV channel along the $E_{\gamma_1} \times E_{\gamma_2}$ valley of the original gated matrices (named C) and of the background subtracted gated matrices (named $A_{b.s.}$), defined by Eq. (1) and listed in Table 1.

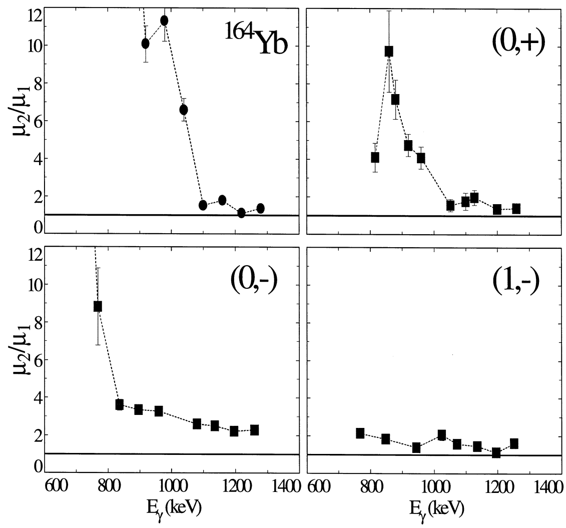

Fig. 6. The ratio $\mu_2(A_{\mathrm{b.s.}})/\mu_1(C)$ obtained from the statistical analysis of the valley of the Total (a) and (α,π) background subtracted gated matrices (b), (c) and (d)), defined by Eq. (1). As one can see, at high transition energies the normalized fluctuations assume values close to 1 (solid line), which is the statistical limit obtained in the case of pure count fluctuations.

covariance between spectra derived from different gating conditions. The covariance provides a measure of the similarity of the cascades feeding into different selected bands. This can in turn be related to the validity of the selection rules associated to the quantum numbers of the intrinsic nuclear structures.

As described in Appendix A, the correlations in fluctuations between two spectra A_1 and A_2 are expressed mathematically by the covariance of counts, defined as

$$\mu_{2,\mathrm{cov}}(A_1,A_2) \equiv \frac{1}{N_{\mathrm{ch}}} \sum_j \langle (M_j - \langle M_j \rangle)(N_j - \langle N_j \rangle) \rangle. \tag{4}$$

Here, M_j and N_j are the number of counts in channel j of the two spectra, which in our case will be obtained by gating on transitions from two different (α,π) configurations. The sum is over a region spanning N_{ch} channels in a two-dimensional sector, and $\langle M_j \rangle$ denotes a local average spectrum (which in our case is found by the routine STATFIT as a numerical smoothed third order approximation of the 2D spectrum). To normalize the covariance, and thereby determine the degree of correlation between the two spectra, the correlation coefficient $r(A_1,A_2)$ is calculated:

$$r(A_1,A_2) \equiv \frac{\mu_{2,\mathrm{cov}}(A_1,A_2)}{\sqrt{[\mu_2(A_1) - \tilde{\mu}_1(A_1)][\mu_2(A_2) - \tilde{\mu}_1(A_2)]}}. \tag{5}$$

While the variance and covariance terms appearing in Eq. (5) are calculated on the final COR background subtracted spectra $A_{b.s}$, defined by Eq. (1) and listed in Table 1, the first moments $\tilde{\mu}_1$ are calculated according to Eq. (3).

The error bars on the correlation coefficient r can also be estimated in terms of variance and covariance of the γ–γ spectra. As shown in Appendix A, after some mathematics one finds the expression

$$\mu_2(r(A_1,A_2)) = \frac{r^2(A_1,A_2)}{N_{\rm ch}}\left[\frac{\tilde{\mu}_1(A_1)\tilde{\mu}_1(A_2)}{(\mu_{2,\,\rm cov}(A_1,A_2))^2} + \frac{(\tilde{\mu}_1(A_1))^2}{2(\mu_2(A_1)-\tilde{\mu}_1(A_1))^2} + \frac{(\tilde{\mu}_1(A_2))^2}{2(\mu_2(A_2)-\tilde{\mu}_1(A_2))^2}\right] + \frac{(1-r^2)^2}{N_{\rm ch}}, \tag{6}$$

where the last term should be replaced by

$$\frac{1}{4n_{\rm ch}}(1-r^2)^2 + \frac{3}{2N_{\rm ch}}(1-r^2)^2$$

for Porter–Thomas fluctuations, which are expected to govern the damping regime [5]. Here $n_{\rm ch}$ denotes the number of channels in one dimension, which is typically 15, and $N_{\rm ch}$ the number of channels in two dimensions, typically 225.

Correlation coefficients (5), measuring directly the similarities between the $A_{1,\rm b.s}$ and $A_{2,\rm b.s}$ spectra, are extracted from the analysis of both the ridge and the valley regions for combinations of the selected configurations, and the results are shown in Fig. 7. The shaded areas in the figures indicate the transition energy region covered by the gate selected transitions, while the lines at $r = 0$ and 1 correspond to the expected values of the correlation coefficient in case of orthogonal or identical path probabilities, respectively (in the sense of Eq. (A.5) of Appendix A). In particular, while the limit $r \to 0$ is expected to be reached when comparing the decay flows at $\approx$ 0 temperature, where the nuclear system is governed by strong selection rules, the opposite limit $r \to 1$ is expected in a compound nucleus regime. For the compound nucleus at sufficiently high temperature, essentially only the parity and signature remain as good quantum numbers of the individual states. The information on the original value of these quantum numbers will subsequently be lost during complicated cascades containing varying numbers of

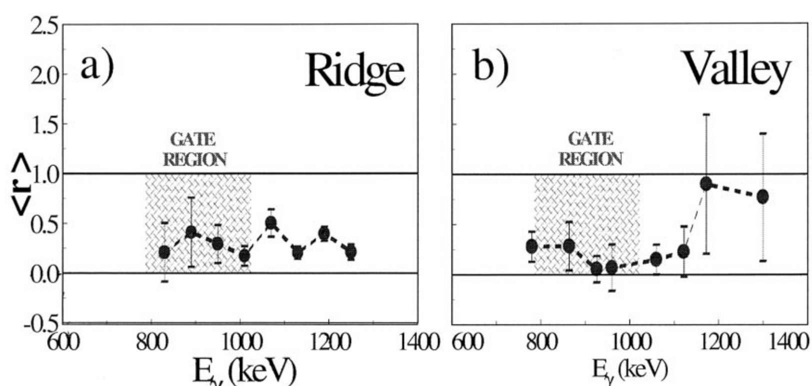

Fig. 7. The average value of the correlation coefficient r, as obtained from the analysis of the ridge (a) and valley (b) regions of the two-dimensional γ – spectrum, for all possible pairs of (α,π) gated spectra. The shaded area indicate the energy intervals covered by the gate-selected peaks.

cooling E1 transitions with different changes of signature. In this compound situation, one will expect that any state can feed democratically the various configurations.

As one can see from Fig. 7a, the average value of the correlation coefficient r, as obtained from the analysis of the ridge structure for all possible pairs of γ–γ spectra gated by the different (α,π) configurations, is found to be positive and of the order of 0.3, for the whole transition energy region. This result indicates that selection rules are important for the cascades among unmixed bands, being obeyed in roughly 70% of the parts of the cascades being investigated, and broken in the remaining 30%. For the low-K bands of ^{163}Er, a correlation coefficient of ≈ 0.3 was also found, while cross-talk between low-K and high-K bands was found to be hindered, displayed by a correlation coefficient close to $r \approx 0$ [7].

As shown in Fig. 7b, the covariance analysis of the valley gives instead a correlation coefficient r close to 0 in the transition energy region covered by the gate-selected γ-rays, while at higher transition energies r seems to assume large positive values, suggesting a stronger sharing of decay paths among cascades which finally feed into different intrinsic configurations. This can be taken as an indication of an approach to a compound situation for the part of the decay which lies at heat energy $\geqslant 1$ MeV, with rotational frequency between 500 and 650 keV, where the damping phenomenon dominates strongly.

3.4. Additivity check on the ridge analysis

The consistency of the results of the fluctuation analysis is checked in the case of the ridge structure through the additivity of the count fluctuations. In fact, on the basis of the experimental values of the correlation coefficient r and of the number of paths $N^{(2)}_{\mathrm{path},i}$, obtained for each specific configuration i from the fluctuation analysis of the ridge structure (shown in average by open circle in the bottom of Fig. 4), one can independently estimate the total number of paths $N^{(2)}_{\mathrm{path,Tot}}$ through the additivity formula

$$\frac{1}{N^{(2)}_{\mathrm{path,Tot}}} = \sum_i \frac{f_i^2}{N^{(2)}_{\mathrm{path},i}} + \sum_{i \neq j} \frac{r(i,j)\, f_i\, f_j}{\sqrt{N^{(2)}_{\mathrm{path},i}\, N^{(2)}_{\mathrm{path},j}}} \tag{7}$$

and compare it with the experimental values shown by closed symbols both in Fig. 4a and Fig. 8. In Eq. (7) f_i represents the relative intensity of configuration i, while $r(i,j)$ is the correlation coefficient, which measures the fraction of common paths between the two configurations i and j.

In the present analysis the relative intensities of the $(0,+)$, $(0,-)$ and $(1,-)$ configurations used in Eq. (7) are extrapolated from the population of the corresponding yrast band (Fig. 1b). They are shown by thin dashed lines in FigIn addition, both the correlation coefficient $r(i,j)$ and the number of paths $N^{(2)}_{\mathrm{path},i}$ for each specific configuration are taken as constant and equal to $\langle r \rangle = 0.3 \pm 0.12$ and $\langle N^{(2)}_{\mathrm{path},i} \rangle = 9.5$, which are the average of the corresponding experimental data shown in Fig. 7a and Fig. 4a, respectively. Inserting these values into Eq. (7) one obtains an average total number of paths falling within the shaded area of Fig. 8a, to be compared with the results obtained assuming no common paths (i.e. $r(i,j) = 0$) or no selection rules associated with the different configurations (i.e. $r(i,j) = 1$), indicated by dashed lines in the figure. As one can see, the experimental data (closed symbols) lie in between these two limits, being

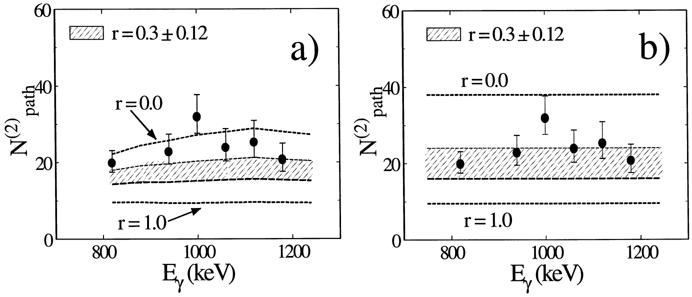

Fig. 8. The number of paths obtained by the fluctuation analysis of the ridge structure of the Total matrix of ^{164}Yb (points in the figure) is compared with the total number of paths independently estimated through the additivity formula (cf. Eq. (7)), assuming no common paths ($r = 0$) or full mixing ($r = 1$) between the different intrinsic configurations (dashed lines in the figures). The shaded area results from a calculation with the correlation coefficient $r = 0.3 \pm 0.12$ including statistical errors, as obtained from the covariance analysis of the ridge structure (see Fig. 7a). In the case of (a) the relative intensities f_i of the specific (α,π) configurations are represented by the population of the corresponding yrast band (as shown in Fig. 1b and Fig. 9), while in the case of (b) the more schematic choice $f_i = 1/4$ has been used.

closer to the $r(i,j) = 0$ regime. This clearly indicates that some paths must be shared between different configurations, allowing for small positive values of the correlation coefficient r, although the experimental value r ≈ 0.3, as obtained from the covariance analysis of the ridges, seems to overestimate the degree of sharing between the different configurations (shaded area in Fig. 8a). One should notice that the choice of the intensities f_i as proportional to the yrast intensities of the corresponding (α,π) combination somehow assumes that all bands with a given parity and signature move up or down in energy together with their yrast representative. This need not be true, and a more schematic choice of the f_i's includes all four (α,π) configurations, with $f_i = \frac{1}{4}$ for each. Using the common value $N^{(2)}_{\mathrm{path},i} = 9.5$ for all four (α,π) configurations one obtains $N^{(2)}_{\mathrm{path,Tot}} = N^{(2)}_{\mathrm{path},i}(\frac{1}{4} + \frac{3}{4}r)^{-1}$, which gives $N^{(2)}_{\mathrm{path,Tot}} = 9.5$ for $r = 1$ and $N^{(2)}_{\mathrm{path,Tot}} = 38$ for $r = 0$. For $r = 0.3 \pm 0.12$ one finds $N^{(2)}_{\mathrm{path,Tot}} = 20 \pm 4$, which agrees better

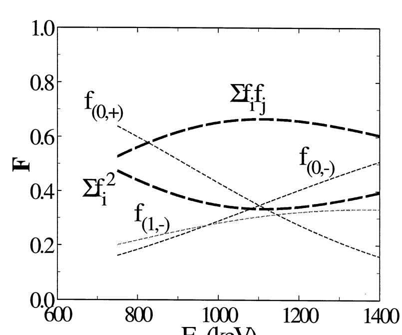

Fig. 9. The relative intensities of the $(0,+)$, $(0,-)$ and $(1,-)$ configurations of ^{164}Yb (thin dashed lines), obtained by interpolation of the population of the corresponding yrast band (see Fig. 1b). The thick solid lines correspond to the quantities Σf_i^2 and $\Sigma f_i f_j$, entering the additivity formula (cf. Eq. (7)).

with the experimental total number of paths, as shown in Fig. 8b. By comparing Fig. 8a and b, one can conclude that the analysis is most sensitive to the correlation coefficient, and not so much to details concerning the choice of the intensities f_i.

Altogether, Fig. 8 displays a consistency between the individual gates and the total gate, giving a strong support to both variance and covariance analysis of the ridges of the gated spectra. A similar additivity check could not be performed in the case of the valley analysis, as a consequence of the large error bars on both the number of paths and the correlation coefficient r.

4. Discussion of results

4.1. Calculated number of paths in ridges and in valley

Since for the first ridge the number of paths gives approximately the number of regular discrete bands [5], the same quantity has been obtained from microscopic cranked shell model calculations including an effective two-body residual interaction of surface delta type (SDI), with standard strength $V_0 = 27.5/\mathrm{A}$ MeV [2]. The lines in the bottom of Fig. 4 display the number of paths obtained from the theory by counting the number of two consecutive transitions having the property that the corresponding branching number n_{branch} is less than 2. The value of n_{branch} gives a measure of the effective number of transitions out of one state, being defined as $n_{\text{branch}}(i) = (\sum_j S_{i,j}^2)^{-1}$, where $S_{i,j}$ is the normalized E2 strength from level i at spin I to level j at spin $(I-2)$. This means that the condition $n_{\text{branch}} < 2$ defines the number of discrete bands at a given spin, before damping sets in. As one can see, the agreement found between data and calculations seems very convincing, both with respect to the total number of discrete bands (solid line) and to the average value over the different (α,π) configurations (dashed line).

The predicted values of $N_{\text{path}}^{(2)}$ based on the same band mixing calculation used for the analysis of the ridge are shown by the full drawn line in Fig. 4b. These theoretical values have been obtained applying the fluctuation analysis technique to the valley region of a simulated spectrum based on the calculated levels and transition probabilities [6]. It has been shown previously that such a simulation is able to reproduce well several features observed in experiments, and in particular the fluctuations. The E2 transition probabilities are calculated microscopically in the region covered by the calculated levels, which extends up to about 2.5 MeV above yrast [2]. At higher energy, the rotational transitions are chosen from a continuous distribution, governed by a rotational damping strength of Gaussian shape, and a width extrapolated from the region of discrete, microscopically calculated levels. The agreement found between data and calculation shows very clearly that the γ transitions populating the valley come from an excitation energy region where the rotational strength must be strongly fragmented. In fact, the calculated levels probed by the valley decay flow show a large branching number $(n_{\text{branch}} \geqslant 10)$, and a spreading width of the E2 strength of the order of 150 keV. This has been taken as the experimental evidence for the rotational damping phenomena [5].

4.2. Calculation and discussion of covariances

In the cascade simulations, gates can also be set on the low lying configurations, corresponding to the experimental gates, and the covariances and correlation coefficient can be evaluated. Fig. 10 displays two examples of such correlation coefficients for the valley fluctuations. A correlation coefficient close to $r = 0$ is found at all transition energies. This is in reasonable agreement with the experimental results up to around 1100 keV of transition energy, but may be in disagreement with the values in the higher energy region, 1200–1300 keV, where the experimental values unfortunately carry large error bars.

The valley fluctuations are mostly sensitive to the energy region of the onset of damping, from about 0.7 MeV to 1.2 MeV of excitation energy above yrast. The selection rules probed by the correlation coefficient are concerned with a segment of the cascade containing about four rotational transitions, which keep the (α,π), together with typically one, possibly two, feeding transitions, which will most probably change the (α,π) quantum numbers. In the simulations, only feeding transitions of E1 multipolarity are included, and for the last feeding transition, stretched transitions dominate. With only one feeding transition, the configurations $(\alpha,\pi) = (0,+)$ will be connected almost exclusively with $(\alpha,\pi) = (1,-)$, and likewise for the other configurations. An occurrence of feeding transitions of M1 character, or maybe some additional possibilities for cooling directly by E2 transitions, will destroy such a strong correlation between the initial and final (α,π)'s of the segment of the cascade. This may be what happens at the higher transition energies in Fig. 7, for which the parts of cascades probed by the correlation coefficient contain about six or seven transitions, and start at slightly higher heat energy.

A less model-dependent view on the behavior of the experimental correlation coefficient of Fig. 7, going from 0 towards 1 with increasing length of the cascades, may be appropriate. The general loss of selection rules displayed by this behavior may be a possible indication of the approach towards a compound situation, connected to the transition between order to chaos in the nuclear many-body system with increasing temperature.

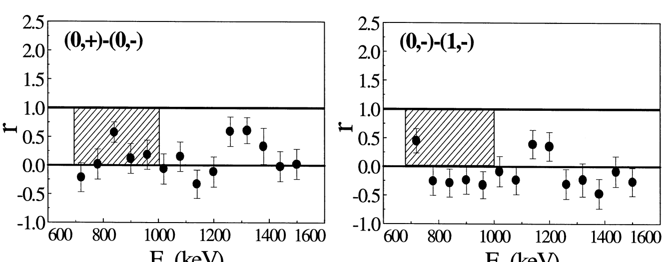

Fig. 10. Examples of the correlation coefficients r extracted from the analysis of the valley region for pairs of simulated spectra gated by the basic configurations $(0,+)$, $(0,-)$ and $(1,-)$ of ^{168}Yb [2,6]. The shaded areas indicate the transition energy regions covered by the gate-selected peaks, which compare with the experimental gating conditions.

5. Conclusions

In the present paper the quasi-continuum $E_{\gamma_1} \times E_{\gamma_2}$ spectrum feeding specific intrinsic configurations of ^{164}Yb is studied making use of variance and covariance fluctuations techniques between pairs of γ–γ matrices. The results of the analysis relative to both ridge and valley structures of the coincidence spectra give quantitative information on the damped rotational motion, in terms of number of decay paths.

First, the additivity rules expected by the fluctuation model have been proved to be well verified by the experimental data, providing a stronger support to this analysis method.

Second, a comparison with the band mixing calculation has been made for the first time on the level of number of paths associated to specific intrinsic configurations. In the case of the ridge structures, the good agreement seen between data and predictions indicates that the selection rules associated with the quantum numbers of the intrinsic structure assumed by the model are valid. Similar results have been obtained in the case of the valley analysis, although one cannot completely rule out their weakening at the moderate excitation energy. Studies with higher counting statistics are necessary to supply a more definitive answer on these points.

Acknowledgements

The support of I.N.F.N. and of the Danish Natural Science Research Council is acknowledged.

Appendix A

A.1. Basic definitions of covariance and correlation coefficient

We consider an energy interval of a two- or three-dimensional gamma spectrum. By setting gates on two different discrete transitions, γ_1 and γ_2, or on transitions along two different low lying rotational bands, two different spectra A_1 and A_2 in the energy interval are produced. The counts in channel j are denoted M_j and N_j, and the interval contains N_{eve} and N'_{eve} gated counts, respectively. The covariance between the two gated spectra A_1 and A_2 is defined by

$$\mu_{2,\mathrm{cov}}(A_1, A_2) \equiv \frac{1}{N_{\mathrm{ch}}} \sum_j \langle \big(M_j - \langle M_j \rangle\big)\big(N_j - \langle N_j \rangle\big) \rangle. \tag{A.1}$$

Most often, the energies of the gating transitions will be situated below the interval in question, and we are interested in the bias introduced by the different coincidence requirements on the cascades, emphasizing some transitions preceeding the gating transition, and weakening others. In the language of the fluctuation analysis [5], the path probabilities will be different with the two gating requirements. By W_i and X_i we

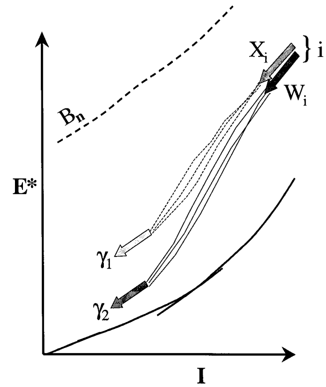

Fig. 11. Schematic illustration in the excitation energy versus spin plane of two decay paths in coincidence with two different γ_1 and γ_2 transitions (gates). The path probabilities are denoted by W_i and X_i, respectively.

denote the path probabilities in coincidence with γ_1 and γ_2, respectively, and the paths and gates are illustrated in Fig. 11.

By the same averaging over binomial distributions as for the second moment [5], one can perform the averaging over counting statistics for the covariance. Since the covariance is linear in both of the gated spectra, the expression for the covariance will contain no term proportional to the first moment μ_1. In this respect the result actually becomes simpler than that of the second moment,

$$\mu_{2,\mathrm{cov}}(A_1, A_2) = \frac{N_{\mathrm{eve}} N'_{\mathrm{eve}}}{N_{\mathrm{ch}}} \times \sum_j \sum_{ii'} \left[\langle W_i X_{i'} P_j(E_i) P_j(E_{i'}) \rangle - \langle W_i P_j(E_i) \rangle \langle X_{i'} P_j(E_{i'}) \rangle \right] \tag{A.2}$$

(with the same notation as Eqs. (4.11)–(4.17) in Ref. [5]). This is to be compared to the equivalent expression for one of the second moments:

$$\mu_2(A_1) = \frac{N_{\mathrm{eve}}^2}{N_{\mathrm{ch}}} \sum_j \sum_{ii'} \left[\langle W_i P_j(E_i) W_{i'} P_j(E_{i'}) \rangle - \langle W_i P_j(E_i) \rangle \langle W_{i'} P_j(E_{i'}) \rangle \right] + \mu_1(A_1). \tag{A.3}$$

Independent of the assumption of transition energy fluctuations, as for discrete bands, or of transition strength fluctuations, as for the Porter–Thomas (PT) distribution, the diagonal terms $i = i'$ of two-step paths or one-step paths will effectively dominate.

To quantify the similarity of the two biased cascades in the two regions, one defines the *correlation coefficient*

$$r(A_1, A_2) \equiv \frac{\mu_{2,\mathrm{cov}}(A_1, A_2)}{\sqrt{\mu_2(A_1) - \tilde{\mu}_1(A_1)} \sqrt{(\mu_2(A_2) - \tilde{\mu}_1(A_2)}} \tag{A.4}$$

(where we have anticipated the influence of the background subtraction by introducing already the notation for the effective first moments $\tilde{\mu}_1$). Averaging over transition energies for the case of ridge fluctuations, one obtains

$$r(A_1, A_2) = \frac{\sum_i W_i X_i}{\sqrt{\sum_i W_i^2}\sqrt{\sum_i X_i^2}} \tag{A.5}$$

and over transition strengths for the case of PT fluctuations:

$$r(A_1, A_2) = \frac{\sum_i W_i X_i + \left(p^{(1)}\right)^2/p^{(2)} \sum_i w_i x_i}{\sqrt{\sum_i W_i^2 + \left(p^{(1)}\right)^2/p^{(2)} \sum_i w_i^2}\sqrt{\sum_i X_i^2 + \left(p^{(1)}\right)^2/p^{(2)} \sum_i x_i^2}}, \tag{A.6}$$

where w_i and x_i refer to one-step paths.

One sees that the correlation coefficient has the appearance of *a scalar product* of normalized path probabilities. This gives a clear intuitive picture. Since all probabilities are positive, the correlation coefficient will always be positive.

Our standard procedures for averaging over realizations have been applied here, by keeping only the diagonal terms $i = i'$ over two- and one-dimensional paths. One may apply the covariance technique also to spectra which are not governed by the same random selections of energies or transition strengths. For example, the occurrence of μ_1 from the counting statistics does not require such random assumptions. However, in order to estimate the statistical significance of r, that is evaluating the error bar $\mu_2(r)$, one needs the random assumptions.

A.2. Second moment of a background subtracted spectrum

In practice, transitions in coincidence with specific gamma rays cannot be selected uniquely. When placing a gate on the transition energy of a specific gamma ray, there will always be a background of transitions below the peak containing the transition.

We consider a spectrum, right-hand side of Fig. 12, which is gated by a peak, superposed on a background, left-hand side of the figure. Usually, we will be interested in two-dimensional spectra, but for illustrative purposes, a one-dimensional spectrum is shown in the figure. The peak is denoted by the letter A, the background by the letter B, and the combined spectrum at the position of the peak by the letter C. It must be assumed that the background under the peak, B_p, introduces the same gating on the gamma-cascades as a wider background next to the peak, B. More precisely, the path probabilities $W_i(B)$ of the background gated spectrum will be the same, independent on whether the coincidence requirement is on the wide gates B or the background B_p underlying the peak.

The background subtracted spectrum $A_{\mathrm{b.s.}}$, gated by the peak A is obtained by subtracting from the spectrum C a scaled background gated spectrum gB

$$A_{\mathrm{b.s.}} = C - gB, \qquad \mu_1(gB) = \mu_1(B_p). \tag{A.7}$$

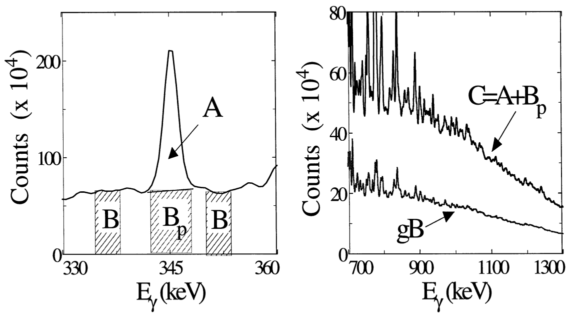

Fig. 12. The right-hand side of the figure shows a spectrum C obtained by gating on a peak A superposed on a background B_p, as schematically illustrated in the left part of the figure. It is assumed that the background under the peak is similar to the background next to the peak, denoted by B. This implies that a background subtracted spectrum $A_{\mathrm{b.s.}}$, gated by the peak A, can be obtained by subtracting a scaled wide background gated spectrum gB, where the scaling factor g is chosen to produce zero background gated counts on the average.

The scaling factor g must be chosen to produce zero background gated counts on the average. But, as we shall see, there is no possibility of getting rid of the pure count fluctuations associated with the background B_p. With path probabilities $W_i(A)$ and $W_i(B)$, the path probability in spectrum C will be:

$$W_i(C) = f_A W_i(A) + f_B W_i(B) \tag{A.8}$$

with f_A and f_B denoting the fractions of the spectrum which are coincident with the peak and the background, respectively.

The fluctuations of the spectrum C has the usual two contributions, one generated by the finite number of paths, and one generated by pure statistical counting fluctuations,

$$\mu_2(C) = \mu_{[2]}(C) + \mu_1(C). \tag{A.9}$$

Here, $\mu_{[2]}(C)$ is quadratic in the number of events, cf. the equivalent definitions (A.11)–(A.13) below, and $\mu_1(C)$ is linear. Further, the quadratic properties of the first term allows us to write

$$\mu_2(C) = \mu_{[2]}(A) + \mu_{[2]}(B_p) + 2\mu_{[2],\,\mathrm{cov}}(A, B_p) + \mu_1(C) \tag{A.10}$$

with

$$\mu_{[2]}(A) = \frac{P^{(2)}}{P^{(1)}} N_{\mathrm{eve}}^2 f_A^2 \sum_i W_i(A)^2, \tag{A.11}$$

$$\mu_{[2]}(B_p) = \frac{P^{(2)}}{P^{(1)}} N_{\mathrm{eve}}^2 f_B^2 \sum_i W_i(B)^2, \tag{A.12}$$

$$\mu_{[2],\,\mathrm{cov}}(A, B_p) = \frac{P^{(2)}}{P^{(1)}} N_{\mathrm{eve}}^2 f_A f_B \sum_i W_i(A) W_i(B). \tag{A.13}$$

Due to the general quadratic dependence, the μ_2 of the scaled wide-gated is scaled by the square of the scaling factor,

$$\mu_2(gB) = g^2 \mu_2(B) = g^2 \mu_{[2]}(B) + g^2 \mu_1(B). \tag{A.14}$$

Applying again general quadratic properties of μ_2, we obtain for the background corrected spectrum

$$\begin{aligned}\mu_2(A_{\mathrm{b.s.}}) &= \mu_2(C) + \mu_2(gB) - 2\mu_{[2],\mathrm{cov}}(C, gB) \\ &= \mu_{[2]}(A) + \mu_{[2]}(B_p) \\ &\quad + 2\mu_{[2],\mathrm{cov}}(A, B_p) + \mu_1(C) + g^2\mu_{[2]}(B) + g^2\mu_1(B) \\ &\quad - 2\mu_{[2],\mathrm{cov}}(A, gB) - 2\mu_{[2],\mathrm{cov}}(B_p, gB). \end{aligned} \tag{A.15}$$

The assumed identity of the two backgrounds B_p and B with respect to affecting the cascade implies the following mathematical identities:

$$\mu_{[2]}(B_p) = g^2\mu_{[2]}(B) = \mu_{[2],\mathrm{cov}}(B_p, gB) \tag{A.16}$$

and

$$\mu_{[2],\mathrm{cov}}(A, B_p) = \mu_{[2],\mathrm{cov}}(A, gB). \tag{A.17}$$

This removes all the unwanted fluctuations due to the transitions in coincidence with the background, to obtain

$$\mu_2(A_{\mathrm{b.s.}}) = \mu_{[2]}(A) + \mu_1(C) + g^2\mu_1(B). \tag{A.18}$$

This final expression shows that the background subtraction is in principle very successful. What remains are: (i) the fluctuations due to paths in coincidences with the peak A, and (ii) the unavoidable fluctuations due to pure counting statistics. One can see that scaling diminishes these fluctuations of the subtracted spectrum.

The same principle goes for spectra which have been subtracted by the COR procedure. Due to the very large number of counts in a COR spectrum, the count fluctuations of the COR spectrum itself will be almost wiped out by the square of the COR scaling factor. However, one has to remember that the first pure counting fluctuation term, $\mu_1(C)$ in the present notation, must always refer back to *the raw spectrum*. It is natural to define the moment relevant for the effective counting statistics, *the effective first moment*,

$$\tilde{\mu}_1(A) \equiv \mu_1(C) + g^2\mu_1(B). \tag{A.19}$$

We now proceed towards the goal of evaluating the variance of the correlation coefficient $\mu_2(r)$. This proceeds through a calculation of the variance of the second moment of a background subtracted spectrum:

$$\mu_2(\mu_2(C - gB)) = \frac{1}{N_{\mathrm{ch}}^2}\left\langle \left\langle \sum_{jj'} M_j^2 M_{j'}^2 \right\rangle - (\langle M^2 \rangle)^2 \right\rangle_{\mathrm{real}}, \tag{A.20}$$

where the subscript ‘‘real’’ denotes averaging over realizations, that is averages over proper samples of transition energies and transition strengths. Carrying out the squares, for example,

$$M_j^2 = M_j(C)^2 - 2gM_j(C)M_j(B) + g^2M_j(B)^2, \tag{A.21}$$

$\mu_2(\mu_2(C - gB))$ splits up into six terms, first three μ_2-type terms

$$\mu_2(\mu_2(C)) + 4g^2\mu_2(\mu_{2,\mathrm{cov}}(C, B)) + g^4\mu_2(\mu_2(B)) \tag{A.22}$$

and next three covariance terms:

$$-4g\,\mu_{2,\,\mathrm{cov}}(\mu_2(C),\mu_{2,\,\mathrm{cov}}(B,C))+2g^2\mu_{2,\,\mathrm{cov}}(\mu_2(C),\mu_2(B))$$
$$-4g^3\mu_{2,\,\mathrm{cov}}(\mu_{2,\,\mathrm{cov}}(C,B),\mu_2(B)). \tag{A.23}$$

There is a specific procedure for evaluating second moments and covariances of second moments and covariances, as illustrated by one example at the end of this appendix. We here quote the results for the three second-moment types,

$$\mu_2(\mu_2(C))=\frac{2}{N_{\mathrm{ch}}}\left[\mu_{[2]}(C)^2+\mu_1(C)^2\right], \tag{A.24}$$

$$4g^2\mu_2(\mu_{2,\,\mathrm{cov}}(C,B))=4g^2\frac{1}{N_{\mathrm{ch}}}$$
$$\times\left[\mu_{[2],\,\mathrm{cov}}(C,B)^2+\mu_{[2]}(C)\,\mu_{[2]}(B)\right.$$
$$\left.+\mu_1(C)\,\mu_1(B)\right], \tag{A.25}$$

$$g^4\mu_2(\mu_2(B))=g^4\frac{2}{N_{\mathrm{ch}}}\left[\mu_{[2]}(B)^2+\mu_1(B)^2\right] \tag{A.26}$$

and for the three covariance-type terms:

$$-4g\,\mu_{2,\,\mathrm{cov}}(\mu_2(C),\mu_{2,\,\mathrm{cov}}(B,C))=-4g\frac{2}{N_{\mathrm{ch}}}\mu_{2,\,\mathrm{cov}}(C,B)\,\mu_{[2]}(C), \tag{A.27}$$

$$2g^2\mu_{2,\,\mathrm{cov}}(\mu_2(C),\mu_2(B))=2g^2\frac{2}{N_{\mathrm{ch}}}\mu_{2,\,\mathrm{cov}}(C,B)^2, \tag{A.28}$$

$$-4g^3\mu_{2,\,\mathrm{cov}}(\mu_{2,\,\mathrm{cov}}(C,B),\mu_2(B))=-4g^3\frac{2}{N_{\mathrm{ch}}}\mu_{2,\,\mathrm{cov}}(C,B)\,\mu_{[2]}(B). \tag{A.29}$$

These expressions are relevant for random transition energies and for wide channels. For more narrow channels, the terms containing second moments acquire the same extra factor as described in Ref. [5] for $\mu_2(\mu_2)$.

It seems a little chaotic with all the terms, but it is worth to point out two aspects of the results: (i) The second moments terms contain a contribution from the counting statistics, whereas the covariances do not. (This seems quite reasonable, but so far it just comes out in the mathematical derivation through cancellations of several terms). (ii) The result $\mu_{2,\,\mathrm{cov}}(\mu_2(C),\mu_2(B))=\frac{2}{N_{\mathrm{ch}}}\mu_{2,\,\mathrm{cov}}(C,B)^2$ has an intuitive interpretation: if the spectra C and B are uncorrelated, that is for the special case $\mu_{2,\,\mathrm{cov}}(C,B)^2=0$, then their second moments will also vary up or down with the realizations independently of each other, which means $\mu_{2,\,\mathrm{cov}}(\mu_2(C),\mu_2(B))=0$.

Combining all terms, one obtains

$$\mu_2(\mu_2(C-gB)) = \frac{2}{N_{\mathrm{ch}}}\Big[\big(\mu_{[2]}(C) - 2g\,\mu_{2,\mathrm{cov}}(C,B)^2 + g^2\mu_{[2]}(B)\big)^2 + \mu_1(C)^2 + 2g^2\mu_1(C)\,\mu_1(B) + g^4\mu_1(B)^2\Big]$$

$$= \frac{2}{N_{\mathrm{ch}}}\big[\mu_{[2]}(A)^2 + \tilde{\mu}_1(A)^2\big], \tag{A.30}$$

which is just what one would expects. The uncertainty in the second moment contains the whole effective counting statistics, including the counting statistics of the original raw spectrum as well as that of the scaled background spectrum.

To evaluate the error bar on the correlation coefficient, one also needs the following second moment:

$$\mu_2(\mu_{2,\mathrm{cov}}(C_1-gB_1, C_2-gB_2)) = \frac{1}{N_{\mathrm{ch}}}\big[\mu_{[2],\mathrm{cov}}(A_1,A_2)^2 + \mu_{[2]}(A_1)\,\mu_{[2]}(A_2) + \tilde{\mu}_1(A_1)\,\tilde{\mu}_1(A_2)\big] \tag{A.31}$$

and the following covariance:

$$\mu_{2,\mathrm{cov}}(\mu_2(C_1-gB_1), \mu_{2,\mathrm{cov}}(C_1-gB_1, C_2-gB_2)) = \frac{2}{N_{\mathrm{ch}}}\mu_{[2]}(A_1)\,\mu_{[2],\mathrm{cov}}(A_1,A_2), \tag{A.32}$$

which follows the same principles.

A.3. Error bar on the correlation coefficient

The correlation coefficient is a function of a covariance and two second moments which for convenience we abbreviate a, b_1 and b_2:

$$r(A_1,A_2) = \frac{\mu_{2,\mathrm{cov}}(A_1,A_2)}{\sqrt{\mu_2(A_1) - \tilde{\mu}_1(A_1)}\,\sqrt{\mu_2(A_2) - \tilde{\mu}_1(A_2)}} = \frac{a}{\sqrt{b_1\,b_2}}. \tag{A.33}$$

Scanning through realizations and counting statistics, variations of these three functions generate the variation of the correlation coefficient:

$$\Delta r = \Delta\left(\frac{a}{\sqrt{b_1\,b_2}}\right) = \frac{\Delta a}{\sqrt{b_1\,b_2}} - \frac{1}{2}\,\frac{a\,\Delta b_1}{\sqrt{b_1^3\,b_2}} - \frac{1}{2}\,\frac{a\,\Delta b_2}{\sqrt{b_1\,b_2^3}} \tag{A.34}$$

from which one obtains

$$\mu_2(r) = \langle (r - \langle r \rangle)^2 \rangle = \left\langle \left(\frac{\Delta a}{\sqrt{b_1 b_2}} - \frac{1}{2} \frac{a\,\Delta b_1}{\sqrt{b_1^3 b_2}} - \frac{1}{2} \frac{a\,\Delta b_2}{\sqrt{b_1 b_2^3}} \right)^2 \right\rangle$$

$$= r^2 \left\langle \left(\frac{\Delta a}{a} \right)^2 + \frac{1}{4} \left(\frac{\Delta b_1}{b_1} \right)^2 + \frac{1}{4} \left(\frac{\Delta b_2}{b_2} \right)^2 - \frac{\Delta a\,\Delta b_1}{ab_1} - \frac{\Delta a\,\Delta b_2}{ab_2} + \frac{1}{2} \frac{\Delta b_1\,\Delta b_2}{b_1 b_2} \right\rangle, \tag{A.35}$$

where the average is over counting statistics as well as realizations.

So, we need to insert from the expressions above,

$$\langle (\Delta a)^2 \rangle = \mu_2(\mu_{2,\mathrm{cov}}(A_1, A_2)), \tag{A.36}$$

$$\langle (\Delta a \Delta b_1) \rangle = \mu_{2,\mathrm{cov}}(\mu_{2,\mathrm{cov}}(A_1, A_2), \mu_2(A_1)), \tag{A.37}$$

$$\langle (\Delta b_1 \Delta b_2) \rangle = \mu_{2,\mathrm{cov}}(\mu_2(A_1), \mu_2(A_2)) \tag{A.38}$$

to obtain

$$\begin{aligned}
\mu_2(r) = {} & r^2 \frac{1}{N_{\mathrm{ch}}} \left[\frac{\mu_{[2],\mathrm{cov}}(A_1, A_2)^2 + \mu_{[2]}(A_1)\,\mu_{[2]}(A_2) + \tilde{\mu}_1(A_1)\,\tilde{\mu}_1(A_2)}{\mu_{[2],\mathrm{cov}}(A_1, A_2)^2} \right] \\
& + r^2 \frac{1}{2N_{\mathrm{ch}}} \left[\frac{\mu_{[2]}(A_1)^2 + \tilde{\mu}_1(A_1)^2}{\mu_{[2]}(A_1)^2} + \frac{\mu_{[2]}(A_2)^2 + \tilde{\mu}_1(A_2)^2}{\mu_{[2]}(A_2)^2} \right] \\
& - r^2 \frac{2}{N_{\mathrm{ch}}} \left[\frac{\mu_{[2]}(A_1)\,\mu_{[2],\mathrm{cov}}(A_1, A_2)}{\mu_{[2]}(A_1)\,\mu_{[2],\mathrm{cov}}(A_1, A_2)} + \frac{\mu_{[2]}(A_2)\,\mu_{[2],\mathrm{cov}}(A_1, A_2)}{\mu_{[2]}(A_2)\,\mu_{[2],\mathrm{cov}}(A_1, A_2)} \right] \\
& + r^2 \frac{1}{N_{\mathrm{ch}}} \left[\frac{\mu_{[2],\mathrm{cov}}(A_1, A_2)^2}{\mu_{[2]}(A_1)\,\mu_{[2]}(A_2)} \right].
\end{aligned} \tag{A.39}$$

Here, the sum of terms containing second moments will be especially simple,

$$r^2 \frac{1}{N_{\mathrm{ch}}} [r^{-2} + 1] + r^2 \frac{1}{2N_{\mathrm{ch}}} [1 + 1] - r^2 \frac{2}{N_{\mathrm{ch}}} [1 + 1] + r^2 \frac{1}{N_{\mathrm{ch}}} r^2 = \frac{1}{N_{\mathrm{ch}}} (1 - r^2)^2. \tag{A.40}$$

This is a natural result: if the two spectra are fully correlated, that is $r = 1$, they will fluctuate up and down together for any realization, so the average over realizations will not contribute any uncertainty.

For PT fluctuations, one has both spike terms and stripe terms to the fluctuations. The result becomes essentially the same, but varies a little according to the relative importance of the two types. One obtains

$$\text{dominating stripes:} \quad \frac{1}{2n_{\mathrm{ch}}}(1-r^2)^2, \tag{A.41}$$

$$\text{dominating spikes:} \quad \frac{1}{N_{\mathrm{ch}}}(1-r^2)^2, \tag{A.42}$$

$$\text{equal importance:} \quad \left[\frac{1}{4n_{\mathrm{ch}}} + \frac{3}{2N_{\mathrm{ch}}}\right](1-r^2)^2, \tag{A.43}$$

where n_{ch} as usual denotes the number of one-dimensional channels. Combining with the counting statistics terms, one obtains

$$\mu_2(r) = \frac{r^2}{N_{\mathrm{ch}}}\left[\frac{\tilde{\mu}_1(A_1)\tilde{\mu}_1(A_2)}{\mu_{2,\mathrm{cov}}(A_1,A_2)^2} + \frac{\tilde{\mu}_1(A_1)^2}{2(\mu_2(A_1)-\tilde{\mu}_1(A_1))^2} + \frac{\tilde{\mu}_1(A_2)^2}{2(\mu_2(A_2)-\tilde{\mu}_1(A_2))^2}\right] + \frac{(1-r^2)^2}{N_{\mathrm{ch}}}, \tag{A.44}$$

where the last term for PT fluctuations should be replaced by one of the expressions (A.41)–(A.43).

As we have seen in Fig. 7, showing the experimental correlation coefficients, the error bars are substantial. To minimize them, one has to select the natural channel width, as derived earlier for the fluctuation analysis [5]. For the background subtraction spectra, the channels could be selected slightly smaller than the natural width, to achieve smaller scaling factors for the background spectra.

A.4. Example of the evaluation of one term

As a typical example of the mathematics of the error bar evaluation, we select the second moment of the covariance $\mu_2(\mu_{2,\mathrm{cov}}(A_1,A_2))$. Following the same line of derivation as for the appendix in Ref. [5], one first writes

$$N_{\mathrm{ch}}^2\,\mu_2(\mu_{2,\mathrm{cov}}(A_1,A_2)) = \left\langle \sum_{jj'} M_j M_{j'} N_j N_{j'} \right\rangle - \sum_{jj'} \langle M_j N_j \rangle \langle M_{j'} N_{j'} \rangle. \tag{A.45}$$

Denoting channel probabilities by Q and R, one obtains

$$\left\langle \sum_{j\neq j'} M_j M_{j'} N_j N_{j'} \right\rangle = N_{\mathrm{eve}}^{[2]} N'^{[2]}_{\mathrm{eve}} \left\langle \sum_{j\neq j'} Q_j Q_{j'} R_j R_{j'} \right\rangle \tag{A.46}$$

and

$$\left\langle \sum_j M_j^2 N_j^2 \right\rangle = \left\langle \sum_j \big(M_j(M_j-1)+M_j \big)\big(N_j(N_j-1)+N_j \big) \right\rangle$$

$$= N_{\rm eve}^{[2]} N'^{[2]}_{\rm eve} \left\langle \sum_j Q_j^2 R_j^2 \right\rangle + N_{\rm eve}^{[2]} N'_{\rm eve} \left\langle \sum_j Q_j^2 R_j \right\rangle$$

$$+ N_{\rm eve} N'^{[2]}_{\rm eve} \left\langle \sum_j Q_j R_j^2 \right\rangle + N_{\rm eve} N'_{\rm eve} \left\langle \sum_j Q_j R_j \right\rangle. \tag{A.47}$$

Combining $j \neq j'$ and j with the simpler term $\sum_{jj'} \langle M_j N_j \rangle \langle M_{j'} N_{j'} \rangle$, one obtains

$$N_{\rm ch}^2\, \mu_2(\mu_{2,\rm cov}(A_1,A_2)) = N_{\rm eve}^{[2]} N'^{[2]}_{\rm eve} \left\langle \sum_{jj'} Q_j Q_{j'} R_j R_{j'} \right\rangle$$

$$- N_{\rm eve}^2 N'^2_{\rm eve} \sum_{jj'} \langle Q_j R_j \rangle \langle Q_{j'} R_{j'} \rangle + N_{\rm eve}^{[2]} N'_{\rm eve} \left\langle \sum_j Q_j^2 R_j \right\rangle$$

$$+ N_{\rm eve} N'^{[2]}_{\rm eve} \left\langle \sum_j Q_j R_j^2 \right\rangle + N_{\rm eve} N'_{\rm eve} \left\langle \sum_j Q_j R_j \right\rangle. \tag{A.48}$$

Inserting *the statistical limit* $Q_j = R_j = 1/N_{\rm ch}$, one has to check the cancellation among eight terms of order of $N_{\rm eve}^4$ or $N_{\rm eve}^3$, to end up with

$$\mu_2(\mu_{2,\rm cov}(A_1,A_2)) = N_{\rm eve} N'_{\rm eve} \left(\frac{1}{N_{\rm ch}} - \frac{1}{N_{\rm ch}^2} \right) \approx \frac{1}{N_{\rm ch}} \mu_1(A_1)\, \mu_2(A_2) \quad \text{stat. limit.} \tag{A.49}$$

Next, we turn to the terms of order $N_{\rm eve}^2 N'^2_{\rm eve}$, approximately equal to

$$\frac{N_{\rm eve}^2 N'^2_{\rm eve}}{N_{\rm ch}^2} \left\langle \sum_{jj'} \left[\left(\sum_{i_1 i_2} W_{i_1} X_{i_2} P_j(E_{i_1}) P_j(E_{i_2}) \right) \left(\sum_{i_3 i_4} W_{i_3} X_{i_4} P_j(E_{i_3}) P_j(E_{i_4}) \right) \right] \right\rangle, \tag{A.50}$$

$$\frac{N_{\rm eve}^2 N'^2_{\rm eve}}{N_{\rm ch}^2} \sum_{jj'} \left[\left\langle \sum_{i_1 i_2} W_{i_1} X_{i_2} P_j(E_{i_1}) P_j(E_{i_2}) \right\rangle \left\langle \sum_{i_3 i_4} W_{i_3} X_{i_4} P_j(E_{i_3}) P_j(E_{i_4}) \right\rangle \right]. \tag{A.51}$$

Here, the important correlations arise when the paths are identical two by two across the pairs $(i_1 i_2)$ and $(i_3 i_4)$, yielding

$$i_1 = i_3 \quad \text{and} \quad i_2 = i_4: \quad \sum_{i \neq i'} W_i^2 X_{i'}^2, \tag{A.52}$$

$$i_1 = i_4 \quad \text{and} \quad i_2 = i_3: \quad \sum_{i \neq i'} W_i X_i W_{i'} X_{i'}. \tag{A.53}$$

The first combination, when inserted, gives rise to a product of two μ_2's, and the second term to the square of the covariance, that is the terms of order $N_{\mathrm{eve}}^2 N'^2_{\mathrm{eve}}$ become

$$\frac{1}{N_{\mathrm{ch}}}\left[\mu_{[2]}(A_1)\mu_{[2]}(A_2)+\mu_{[2],\mathrm{cov}}(A_1,A_2)^2\right], \tag{A.54}$$

where it actually does not matter whether we write $\mu_{[2],\mathrm{cov}}$ or $\mu_{2,\mathrm{cov}}$, since there are no μ_1 terms contributing to $\mu_{2,\mathrm{cov}}$. Collecting both terms of the order of $N_{\mathrm{eve}}^2 N'^2_{\mathrm{eve}}$ and $N_{\mathrm{eve}} N'_{\mathrm{eve}}$, we finally obtain

$$\begin{aligned}&\mu_2(\mu_{2,\mathrm{cov}}(A_1,A_2))\\ &\quad=\frac{1}{N_{\mathrm{ch}}}\left[\mu_{[2]}(A_1)\mu_{[2]}(A_2)+\mu_{[2],\mathrm{cov}}(A_1,A_2)^2+\mu_1(A_1)\mu_1(A_2)\right].\end{aligned} \tag{A.55}$$

References

[1] B. Lauritzen, T. Døssing, R.A. Broglia, Nucl. Phys. A 457 (1986) 61.
[2] M. Matsuo, T. Døssing, E. Vigezzi, R.A. Broglia, K. Yoshida, Nucl. Phys. A 617 (1997) 1.
[3] S. Leoni, B. Herskind, T. Døssing, P. Rasmussen, P. Bosetti, A. Bracco, S. Frattini, M. Matsuo, N. Nica, E. Vigezzi, A. Atac, M. Bergström, A. Brockstedt, H. Carlsson, P. Ekström, F. Ingebretsen, H.J. Jensen, J. Jongman, G.B. Hagemann, R.M. Lieder, T. Lönnroth, A. Maj, B. Million, A. Nordlund, J. Nyberg, M. Piiparinen, H. Ryde, D.C. Radford, M. Sugawara, P.O. Tjøm, A. Virtanen, Nucl Phys. 587 (1995) 513.
[4] B. Herskind, A. Bracco, R.A. Broglia, T. Døssing, A. Ikeda, S. Leoni, J. Lisle, M. Matsuo, E. Vigezzi, Phys. Rev. Lett. 68 (1992) .
[5] T. Døssing, B. Herskind, S. Leoni, A. Bracco, R.A. Broglia, M. Matsuo, E. Vigezzi, Phys. Rep. 268 (1996) 1.
[6] A. Bracco, P. Bosetti, S. Frattini, E. Vigezzi, S. Leoni, T. Døssing, B. Herskind, M. Matsuo, Phy. Rev. Lett. 76 (1996) 4484.
[7] P. Bosetti, S. Leoni, A. Bracco, B. Herskind, T. Døssing, G.B. Hagemann, R. Bark, A. Brocksted, P. Ekström, H. Carlsson, A. Nordlund, H. Ryde, F. Camera, S. Frattini, M. Mattiuzzi, B. Million, D. Bazzacco, R. Burch, G. de Angelis, D. De Acuna, M. de Poli, P. Pavan, Phy. Rev. Lett. 76 (1996) 1204.
[8] S. Leoni, A. Bracco, T. Døssing, B. Herskind, J.C. Lisle, M. Matsuo, E. Vigezzi, J. Wrzesinski, Eur. Phys. J. A 4 (1999) 229.
[9] R.U. Haq, A. Pandey, O. Bohigas, Phy. Rev. Lett. 48 (1982) 1086.
[10] O. Bohigas, H.A. Weidenmüller, Ann. Rev. Nucl. Part. Sci. 38 (1988) 421.
[11] B.R. Mottelson, Nucl. Phys. A 557 (1993) 717c.
[12] S. Frattini, A. Bracco, S. Leoni, F. Camera, B. Million, N. Blasi, G. Lo Bianco, M. Pignanelli, E. Vigezzi, B. Herskind, T. Døssing, M. Bergström, P. Varmette, S. Törmänen, A. Maj, M. Kmiecik, D.R. Napoli, M. Matsuo, Phys. Rev. Lett. 83 (1999) 5234.
[13] C.W. Beausang, D. Prevost, M. Bergström, G. de France, B. Haas, J.C. Lisle, C. Theisen, J. Timar, P. Twin, J. Wilson, Nucl. Inst. Methods Phys. Res. A 364 (1995) 560.
[14] G.B. Hagemann et al., to be published.
[15] D.C. Radford, Nucl. Inst. Meth. A 361 (1995) 297.
[16] O. Andersen, J.D. Garrett, G.B. Hagemann, B. Herskind, D.L. Hillis, L.L. Riedinger, Phys. Rev. Lett. 43 (1979) 10.
[17] B. Million, S. Leoni, A. Bracco, J. Moretti, S. Frattini, P. Bosetti, F. Camera, M. Mattiuzzi, B. Herskind, R.A. Bark, I. Bearden, G.B. Hagemann, H.J. Jensen, Phys. Lett. B 415 (1997) 321.
[18] S. Frattini, A. Bracco, S. Leoni, P. Bosetti, B. Herskind, T. Døssing, M. Bergström, G.B. Hagemann, H. Ryde, J.P. Vivien, A. Bagshow, D. Smalley, A.G. Smith, Phys. Rev. Lett. 81 (1998) 2659.